PHYSOR 2004 -The Physics of Fuel Cycles and Advanced Nuclear Systems: Global Developments
Chicago, Illinois, April 25-29, 2004, on CD-ROM, American Nuclear Society, Lagrange Park, IL. (2004)

Localized Void Feedback Effects under Single Rod Drop Transient in BWR

Akitoshi Hotta [*1] Hiroshi Shirai[1] and Shinya Mizokami [2]
[1]*TEPCO Systems Corporation, Shinbashi, Minato-ku, Tokyo, Japan, 105-0004*
[2]*TEPCO, Uchisaiwai-cho, Chiyoda-ku, Tokyo, Japan, 100-8560*

A postulated single control rod drop transient was analyzed for a typical BWR plant. In order to include feedback effects of the intra-bundle void distribution in those bundles neighboring the withdrawn control blade, transient pin power distributions were reconstructed by the plant simulator TRAC/BF1-ENTRÉE and were exported to the subchannel code, NASCA.

The cross section libraries with flat and distorted void distributions were combined in the two-way coupling calculation. Exposure trends of neutronic properties were compared between two void distributions. Although the infinite multiplication factor wasn't notably influenced, the radial peaking factor changed significantly due to void distortions. A pin-by-pin concentration change of fissile materials also contributes to this result.

At the initial state, the void fraction in peripheral subchannels facing the withdrawn blade became prominently low. The power level in the surrounding bundles decreased due to larger neutron leakage caused by distorted void distributions. During transient, the linear power density at the critical fuel rod increased faster than that of the flat void model. Change in the fuel surface heat flux was attenuated due to the heat conduction time delay. The peak cladding temperature was slightly lower than that of the flat void model due to cancellation among these factors.

KEYWORDS: ENTRÉE, NASCA, TRAC/BF1, Control Rod Drop, Void Distortion, BWR, Two-way Coupling, Subchannel Code, Void Drift

1. Introduction

In the authors' previous study based on a realistic turbine trip scenario, results of the one-way coupling calculation between the plant simulator and the subchannel code have been reported. Feedbacks of the detailed intra-bundle void distortion were ignored in this study.[1] Under the core-wide reactivity insertion initiated at nearly all-rods-out (ARO) states, it was confirmed that transient void distribution remained sufficiently uniform in the upper part of bundles where the boiling transition would occur.

On the other hand, if a certain control blade is deeply inserted at the initial state, the pin power distribution in neighboring bundles is conspicuously distorted and the void fraction becomes low in the corner and side subchannels facing this control blade. When this control blade is suddenly withdrawn, the highly localized reactivity will be inserted. This distorted void distribution will be maintained during first a few seconds of this transient due to the fuel heat conduction delay as observed in the turbine trip event. In order to estimate its impact precisely, it is necessary to include feedback effects of detailed void distributions in the cross section and other neutronic properties.

The terminology *subchannel* stands for the flow path formed by neighboring fuel rods and channel walls in the nuclear fuel bundle. The BWR subchannel code is made up from numerical models designed for analyzing the detailed two-phase fluid dynamics inside the fuel bundle. Proper treatment of the

* Corresponding author, Tel. 81+3+4586+6742, FAX 81+3+4586+1190, E-mail: hotta-akitoshi@tepsys.co.jp

subchannel-scale vapor mobility is indispensable in this study. For this end, it is required to implement numerical models describing the vapor-liquid cross flow through gaps between fuel rods. Under today's computer circumstances, it seems premature to perform the whole core calculation with assigning subchannel modules for each fuel bundle. Instead, the off-line simplified two-way coupling methodology will be proposed in the subsequent sections. The previous methodology applied in the turbine trip event needs to be extended[1] so as to include feedback effects of the intra-bundle void distortion on the cross sections and other neutronic properties.

2. Calculation Procedure

2.1 Event Scenario

The plant condition was defined based on the second point of the turbine trip test performed at the Peach Bottom unit 2.[1] The control blade G indicated in Fig.1 was deeply inserted (4/48) and it was postulated to be withdrawn at the design velocity of 95(cm/sec). The four surrounding bundles consisted of one 8x8 and three 7x7 bundles.

Since a realistic core-loading pattern was assumed here, the maximum worth of control blades was not so large. Under postulated conditions where the worth becomes close to 1$, impacts of this void distortion on the local peaking factor or the peak cladding temperature will be worth being examined. The present study will supply some useful guidelines how to account for positive and negative factors contributing to the cladding temperature from a numerical point of view.

2.2 Numerical Models

Figures 2 shows the information flow connecting the plant simulator, TRAC/BF1[2]-ENTRÉE[3] and the subchannel code NASCA[4]. The two-fluid model is employed in both TRAC/BF1 and NASCA and this combination makes this coupling system applicable to a wide range of slow and fast transients. An efficient transient pin power reconstruction algorithm is implemented in ENTRÉE, which realizes the detailed pin-by-pin neutronic-thermalhydraulic coupling calculation at the practical cost. Furthermore, the advanced vapor-liquid cross flow models implemented in NASCA meet the main objective of this study.

Excluding the core region, the nodalization employed in TRAC/BF1 was the one applied in the OECD/NEA turbine trip benchmark.[1] The major component libraries were the VESSEL module for a vessel and its associated internals, the SEPD module for the steam separator and dryer, the PUMP module for the pump and its associated loop and the JETP module for the jetpump consisting of driveline, nozzle, throat, diffuser and discharge. A combination of the PIPE (One-dimensional duct), the VALVE(One-dimensional restricted flow) and the BREAK(Pressure boundary) modules represented the pressure propagation in the main steam line up to the turbine control valve and the bypass valve. A combination of the PIPE and the FILL(Velocity and temperature boundary) modules represented the outlet of the feedwater line.

The core was represented by the CHAN modules that represent the one-dimensional fuel bundle and channel walls. In mapping the core thermal-hydraulic regions, all the fuel bundles were ranked according to their power level, bundle type and orifice type and they were grouped into fifty regions of the nearly equal region integrated power level. As shown in Fig.1, the additional eight regions were concentrated in the focused zone in order to take into account the localized perturbation of thermal-hydraulic states around the withdrawn control blade.

In ENTRÉE, the three-dimensional neutron diffusion equation is solved by the two-group nodal expansion method based on the Legendre semi-analytical functions.[3] The transient pin-power

reconstruction method is the one proposed by Rempe where the basic pre-requisite is separability of the intra-bundle power distribution into the homogeneous and heterogeneous components.[5]

NASCA is the advanced two-fluid/three-field subchannel code. In addition to the continuous liquid and vapor phases, this code explicitly considers the droplet phase. The cross flow is decomposed into the three independent components, (1) the divergence, (2) the turbulent mixing and (3) the void drift. The diffusion type void settlement model proposed by Lahey[6] is employed for Components (2) and (3). The three components have been separately quantified through a series of air-water tests performed using communicated parallel channel systems at the Kumamoto University.[7] It is known that the turbulent mixing and the void drift manifest themselves in the slug and churn flow regimes. According to observation by Sadatomi and Kawahara, this dependence on the two-phase flow regime is macroscopically expressed as the two-phase factor of a function of the void fraction.[8] The diffusion coefficient in the void settlement model is multiplied by this factor.

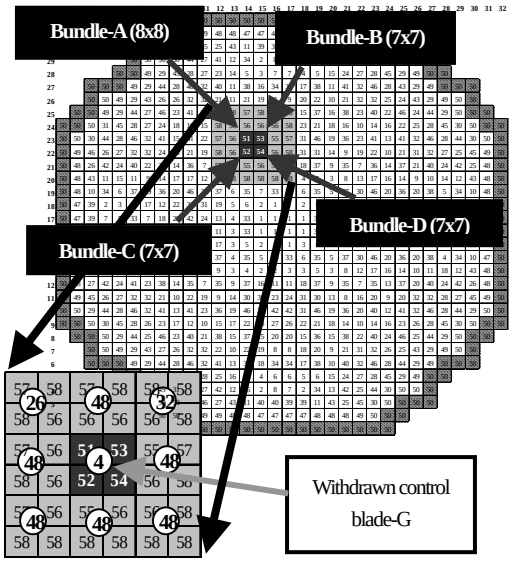

Fig.1 Core map and focused zone (48:Fully withdrawn)

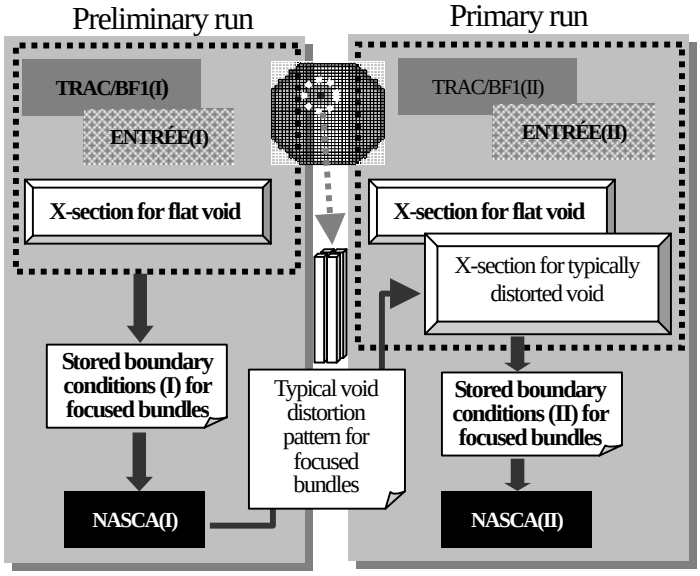

Fig.2 Local core off-line two-way coupling method applied in this study

2.3 Local Core Off-line Two-way Coupling Method

Detailed two-phase fluid dynamics was analyzed by NASCA in the four surrounding bundles denoted as A to D in Fig.1. In the core modeling, the twenty-six axial nodes were commonly employed in TRAC/BF1(CHAN modules), ENTRÉE and NASCA. Single bottom and upper reflector nodes were also included in these nodes. The transferred boundary conditions were (1) the mass flow and temperature at the channel inlet, (2) the pressure at the channel outlet evaluated by TRAC/BF1, (3) the pin power distribution evaluated by ENTRÉE and (4) the detailed void distribution evaluated by NASCA.

The two-way coupling procedure is composed of the two steps, the preliminary and the primary run. In the preliminary run, the entire core region is analyzed by TRAC/BF1(I)-ENTRÉE(I) based on the flat void cross sections. The boundary conditions (1)-(3) are once saved and they are given to NASCA(I). Those bundles belonging to the focused zone are analyzed by NASCA(I) in order to know typical void distribution patterns applicable to this event. Based on the conventional format, a set of cross section libraries is prepared for each of these typical void distributions. In the primary run, these multiple cross section libraries are assigned to the focused bundles while the flat void cross section library is assigned in the rest of the core. The whole core calculation is again analyzed by

TRAC/BF1(II)-ENTRÉE(II). The boundary conditions (1)-(3) are again saved and they are given to NASCA(II) in order to produce the final solution.

3. Production of Cross Section with Void Distortion

3.1 Typical Void Distortion Pattern in Focused Bundles

In the preliminary run, the postulated scenario was analyzed based on the flat void cross sections. Figures 3 shows three typical void patterns for Bundle-A (8x8) observed at the 15-th, 20-th and 25-th nodes under the initial state. The planar average void fractions of Bundles-B, C and D are lower than those of Bundle-A due to their smaller power density. It can be seen that the general pattern depends mainly on the average void fraction: i.e. as the average void fraction becomes smaller, the void distribution will be more sharply distorted. After summarizing trends of the four bundles, it can be roughly assumed that there is analogy in the void distortion patterns among the same bundle type (7x7 or 8x8). Hence, the shapes shown in Fig.3 were applied to Bundle-A while those shapes estimated for Bundle-D were applied to Bundles-B, C and D.

In producing macroscopic cross section libraries, a series of exposure calculations was performed based on the detailed lattice transport model at the four discrete historical void fractions of (0%, 20%, 40%, 70%). From each historical void case, a set of instantaneous changes was branched off to the void fractions at (0%, 20%, 40%, 70%), the control blade insertion and the fuel temperature rise. The patterns I, II and III shown in Figs.4 and 5 were applied to the above-mentioned historical and instantaneous void fraction cases of 20%, 40% and 70%, respectively.

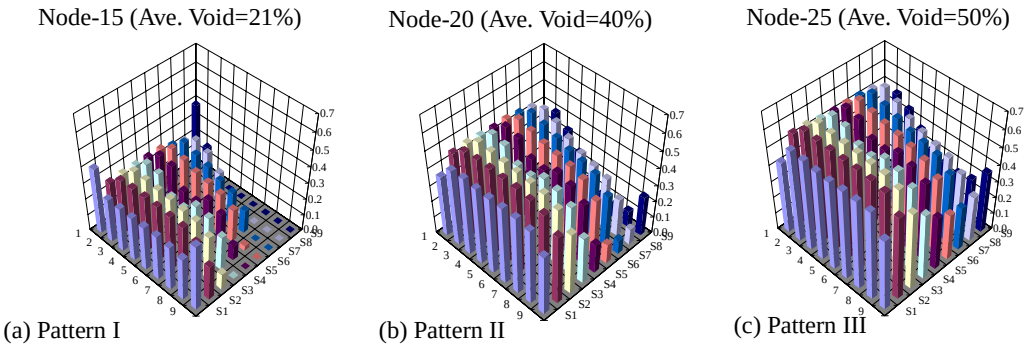

Fig. 3 Typical void distortion patterns observed in 8x8 type bundle-A (8x8 Type)

3.2 Results of Lattice Calculation

The result of lattice calculation was compared between the flat void and the distorted void cases. Figure 4 exemplifies exposure trends of the infinite multiplication factor for a segment allocated in the middle part of Bundle-A. It can be seen that the segment-scale neutron balance would not be affected so much by localized void distortions. Figure 5 shows the local peaking factor for the same segment. As anticipated, the local peaking factor will be significantly affected. The magnitude of influences depends on the average void fraction and the exposure. The local peaking factor will be increased more as the average void fraction becomes larger. If the void fraction becomes smaller than 20%, the two cases will converge to the equivalent level for the exposure beyond 10(GWD/T). If the void fraction becomes larger than 40%, the local peaking factor of the distorted void case remains always larger than that of the flat void case.

Detailed examinations on the pin-by-pin concentration of fissile materials were performed. Under distorted void conditions, the moderator density becomes significantly higher in the

wide gap region than that in the narrow gap region. Skew in the moderator density distribution modifies a shape of the neutron spectra inside the bundle. U235 will be consumed faster in the wide gap region. Pu239 will be also produced faster in the wide gap but is consumed faster at the same time because of the harder local neutron spectra. As a result of this localized exposure process, the peak rod location will be moved differently.

In case of the 7x7 type, it should be noted that void distortions became slightly steeper due to its larger cell size. This resulted in slightly larger influences on the local peaking factor. However essentially analogous trends were observed in those 7x7 type segments belonging to Bundle D.

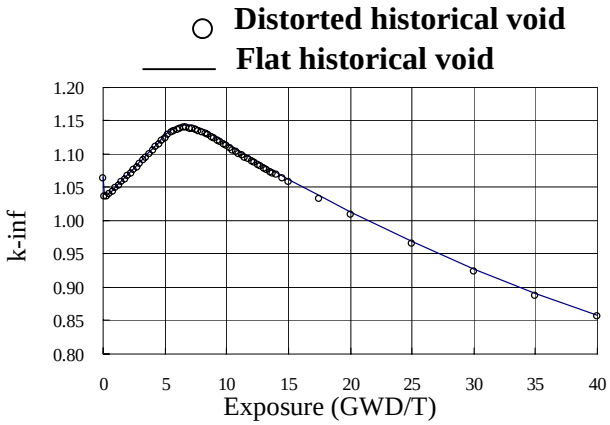

Fig.4 Infinite multiplication factor for middle segment of 8x8 types at void fraction of 40%

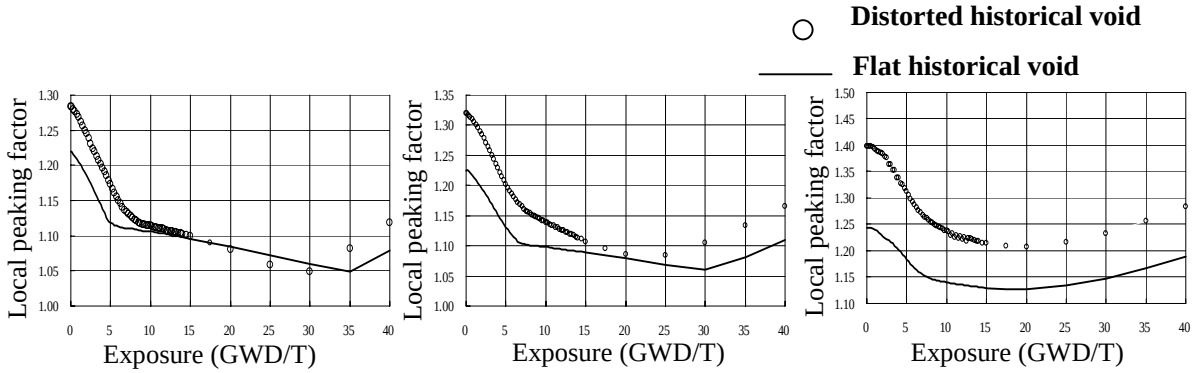

(a) α_{his} =20% (b) α_{his} =40% (c) α_{his} =70%

Fig.5 Local peaking factor for middle segment of 8x8 type at various void fractions

4. Results of Coupled Calculation

4.1 Steady-State Results

The two coupling runs, preliminary and primary, were compared. As described in Section 2.3 and Fig.2, the only flat void cross section library was employed in the preliminary run. In the primary run, the distorted void cross sections were assigned solely in the four focused bundles while the flat void cross sections were employed in the rest of the core.

Table 1 summarizes the initial state radial power distribution in the focused zone predicted by the above-mentioned two methods. In those bundles surrounding the control blade, the power level predicted by the primary run was slightly lower than that by the preliminary run. This comparison suggests that the void distortion would enhance localized neutron leakage from the focused zone. In fact, there were several control cells in this core where control blades were deeply inserted. Similar void distortions and local neutron leakage flows also existed at these zones. Under this single rod drop event, major transient processes will be dominated by the localized power rising at the withdrawn control cell. Hence the above-mentioned neutron leakage at distant spots can be regarded as the secondary factor.

Table 1 Comparison of steady-state core average radial power distributions
in focused zone between preliminary and primary runs

Preliminary run						Primary run					
Row/Col	12	13	14	15	16	Row/Col	12	13	14	15	16
25	1.259	1.051	1.271	1.019	0.962	25	1.252	1.044	1.262	1.011	0.956
24	1.059	1.051	1.010	0.985	0.934	24	1.053	1.043	0.999	0.971	0.926
23	1.326	1.053	**0.854**	0.726	1.107	23	1.318	1.043	**0.840**	0.676	1.093
22	1.125	1.095	0.762	0.746	0.982	22	1.118	1.080	0.713	0.702	0.970
21	1.404	1.158	1.260	1.057	1.068	21	1.398	1.151	1.246	1.045	1.062

4.2 Transient Results

Figure 6 shows snapshots of the radial power distribution at the 5-th node predicted by the primary run (TRAC/BF1(II)-ENTRÉE(II)). A steep power peak appeared just after passing of the control blade. Then this power peak was slightly lowered and the core maintained this power distribution in the steady-state. Almost identical results were confirmed in the preliminary run.

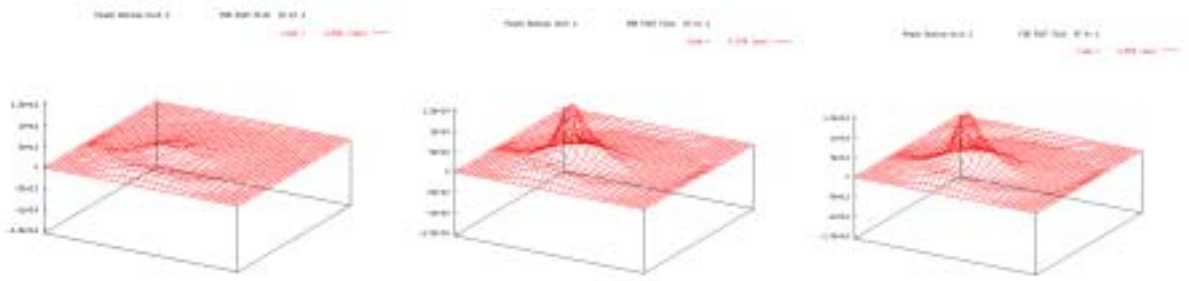

(a) 0.5 seconds (b) 2.0 seconds (c) 2.5 seconds

Fig.6 Snapshots of core radial power distribution at Node-5
in primary coupled run (measured from initial power level)

Figures 7 and 8 display transition of the pin power distribution in the focused zone evaluated by ENTRÉE(II) and the intra-bundle void distribution of Bundle-A evaluated by NASCA(II), respectively. These figures prove that the pin power distribution will change instantaneously while the void distribution will exhibit little change until the bundle experienced its peak power. Figure 9 shows history of the peak linear power density of Bundle-A. The initial power level predicted by the primary run was smaller than that by the preliminary run. This disagreement can be attributed to larger neutron leakage in the former method. During withdrawal of the control blade, the linear power density rose more rapidly in case of the primary run and the two methods approached toward the equivalent level.

Finally the peak cladding temperature is compared in Fig.10. Under rapid transients like this example, the peak value will be reached before the accumulated heat is released from fuel rods. Hence it can be roughly assumed that the cladding temperature is proportional to the time integration of power density curves shown in Fig. 9. Quantitatively, the estimated peak cladding temperature was lowered only by 0.4 Kelvin for the primary run. This result was mainly caused by cancellation between the intra-bundle radial peaking factor increase (positive) and the inter-bundle neutron leakage effect (negative). The remaining difference in the linear power density shown in Fig. 12 will be further attenuated by the fuel heat conduction time delay.

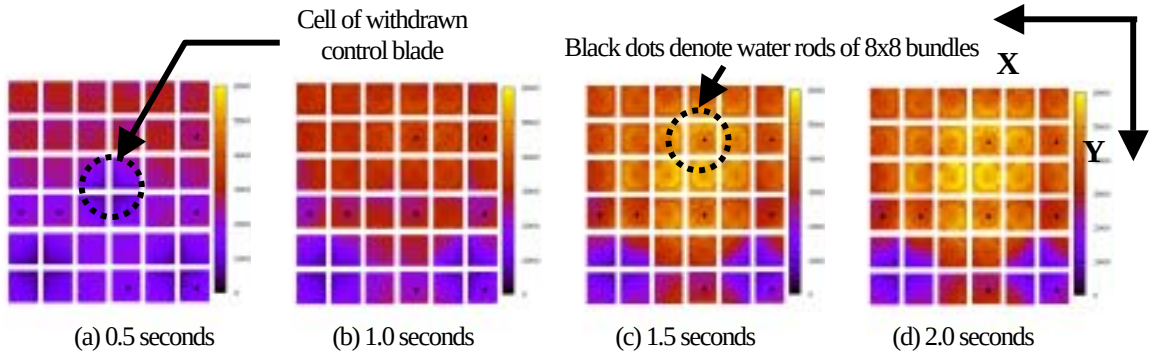

Fig.7 Transient pin power in focused zone reconstructed in primary run

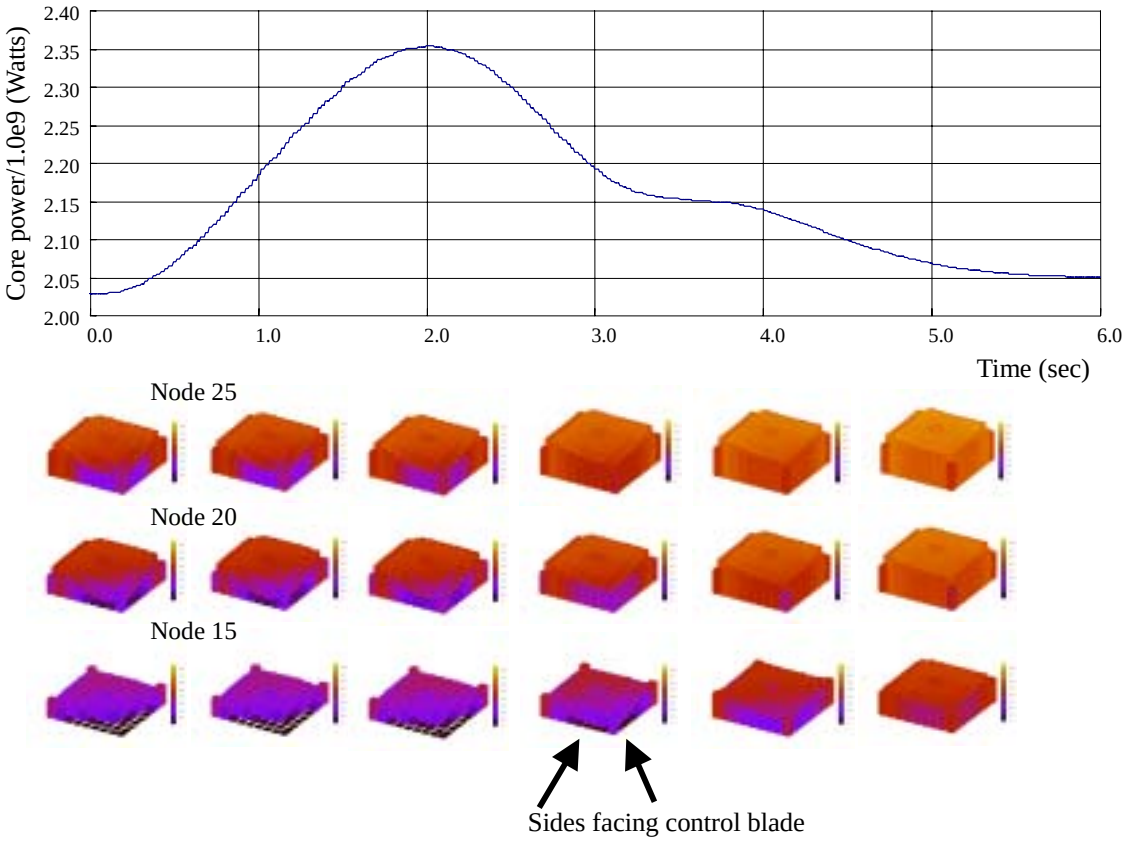

Fig.8 Transition of core power and void distributions of Bundle-A in primary coupled run

The control blade drop transient is supposed to be the most susceptible event against the void distortion. Although the presented results were favorable from a design point of view, it must be also noted that the coupling calculation including a subchannel code is the state-of-the-art technology. The subchannel modeling itself is a still developing field of which prediction of void distributions (clarification of cross flow mechanisms) remains one of the major academic subjects. A numerical treatment of microscopic feedback mechanisms between neutronics and two-phase fluid dynamics is another important subject. It is desired that quality of these coupling calculations will be improved in accordance with advancements in these relevant fields.

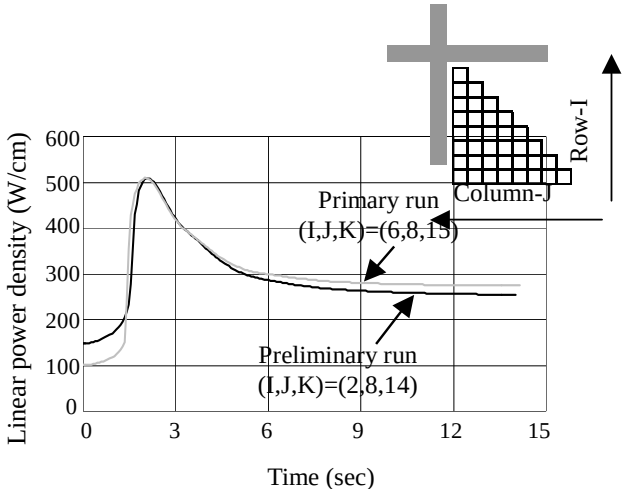

Fig. 9 Comparison of linear power density history of Bundle-A

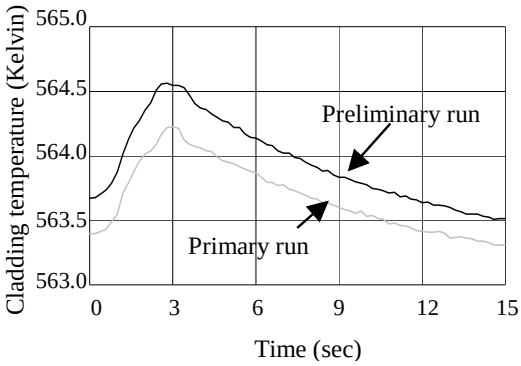

Fig. 10 Comparison of peak cladding temperature history of Bundle-A

5. Conclusion

(a) Under the one rod drop transient, it is possible to assume typical void distortion patterns in those bundles surrounding the withdrawn control blade. Under these typical void distortions, the segment-scale neutron balance would not be affected so much. On the other hand, the local peaking factor will be increased significantly.

(b) The off-line two-way coupling procedure composed of the two-step calculations was proposed. In the preliminary run, the entire core region is analyzed by TRAC/BF1-ENTRÉE based on the flat void cross sections. Typical void distribution patterns of those bundles belonging to the focused zone were analyzed by NASCA. In the primary run, the distorted void cross section libraries were assigned to the focused bundles and the whole core calculation is again analyzed by TRAC/BF1-ENTRÉE. The channel boundary conditions were given to NASCA in order to produce the final solution.

(c) In the coupling calculation, it was shown the void distortion would enhance localized neutron leakage from the focused zone surrounding the withdrawn control blade. The initial state radial power distribution indicated the power level of the primary run was slightly lower than that of the preliminary run due to this enhanced neutron leakage.

(d) In the primary run, the estimated peak cladding temperature was lowered only by 0.4 Kelvin. This result was mainly caused by cancellation between the intra-bundle radial peaking factor increase (positive) and the inter-bundle neutron leakage effect (negative). The remaining difference in the linear power density will be further attenuated by the fuel heat conduction time delay.

Acknowledgements

This study was funded by Tokyo Electric Power Company (TEPCO), Japan.

References

1) A. Hotta, "Application of TRAC/BF1-ENTRÉE-NASCA to OECD NEA/NSC BWR Turbine Trip Benchmark", *to be published in Nucl. Sci. Eng.*
2) W. H. Rettig and N. L. Wade, "TRAC-BF1/MOD1: An Advanced Best-Estimate Computer Program for BWR Accident Analysis", *NUREG/CR-4356*(1992).
3) A. Hotta, H. Ninokata and A. J. Baratta, "Peach Bottom 2 Turbine Trip Simulation by Coupling System of 3D Nodal Code ENTRÉE and TRAC-BF1", *Int. Topical. Mtg. on Math. and Comp., September* 27-30, 1804(1998).

4) H. Ninokata , M. Aritomi, N. Anegawa et *al., Proceeding of 4th International Seminar on Subchannel Analysis, ISSCA-4*, Tokyo, 231(1997).
5) K. Rempe, K. Smith, A. F. Henry , *Nucl. Sci. Eng.*, 103, 334(1989).
6) R. T. Lahey and F. T. Moody, "The Thermal-Hydraulics of A Boiling Water Nuclear Reactor", *Second Edition, ANS* ,(1993).
7) M. Sadatomi, " Study of Single- and Two-Phase Fluid Transfer Between Subchannels at Kumamoto University," to be presented at NUTHOS-6 (2004).
8) A. Kawahara, "Fundamental study on inter-subchannel exchange of fluids in a BWR fuel rod bundle", *Ph.D. Thesis, Department of Mechanical Engineering, Kumamoto University,* (1998).